Improved Capacity Retention of SiO$_2$-Coated LiNi$_{0.6}$Mn$_{0.2}$Co$_{0.2}$O$_2$ Cathode Material for Lithium-Ion Batteries

Xiaoxue Lu [1,2,3], **Ningxin Zhang** [1], **Marcus Jahn** [1,*], **Wilhelm Pfleging** [2,3] and **Hans J. Seifert** [2]

[1] Business Unit of Electric Drive Technologies, Center for Low-Emission Transport, Austrian Institute of Technology GmbH, Giefinggasse 2, 1210 Vienna, Austria

[2] Institute for Applied Materials–Applied Materials Physics (IAM-AWP), Karlsruhe Institute of Technology, Hermann-von-Helmholtz-Platz 1, 76344 Eggenstein-Leopoldshafen, Karlsruhe, Germany

[3] Karlsruhe Nano Micro Facility (KNMF), 76344 Eggenstein-Leopoldshafen, Karlsruhe, Germany

* Correspondence: marcus.jahn@ait.ac.at

check for updates

Abstract: Surface degradation of Ni-enriched layered cathode material Li[Ni$_{0.6}$Mn$_{0.2}$Co$_{0.2}$]O$_2$ (NMC622) is the main reason that leads to large capacity decay during long-term cycling. In the frame of this research, an amorphous SiO$_2$ coating was applied onto the surface of the commercially available NMC622 powder by a wet coating process, through the condensation reaction of tetraethyl orthosilicate. The chemical composition of the coating layer was analyzed by inductively-coupled plasma. The morphology was studied by scanning electron microscopy and transmission electron microscopy. Electrochemical properties, including cyclic voltammetry, galvanostatic cycling, and rate capability measurements in a half-cell configuration, were tested to compare the electrochemical behavior of the non-coated and coated NMC622 materials. It is shown that the rate performance of the NMC622 materials is not affected by the coating layer. After 700 cycles in the range of 3.0–4.3 V at 2 C discharge, the cells with SiO$_2$-coated NMC622 materials retained 80% of their initial capacity, which is higher than the uncoated ones (74%). Physicochemical characterizations, e.g., XRD and SEM, were performed post-mortem to reveal the stabilizing mechanism of the SiO$_2$-coated NMC622 electrodes after long-term cycling. Based on these results, this is due to the shielding effect of the coating between the NMC622 particle surface and the liquid electrolyte, along with its scavenging effect on HF. SiO$_2$ coating is therefore a facile surface modification method that results in potentially significant enhancement of the cyclic stability of Ni-rich NMC materials.

Keywords: lithium-ion battery; Ni-rich layered cathode material; SiO$_2$ coating; capacity retention

1. Introduction

Electric vehicles (EVs) and plug-in hybrid electric vehicles (PHEVs) have developed rapidly in recent years. The problems which people are most concerned with are driving distance, battery life, and safety, namely reliability of battery. Cathodes and anodes, as the most important parts of a battery, are two of the research focuses. Compared to anode materials, cathode materials have relatively lower specific capacity and twice as high a price [1]. Therefore, the key to increasing energy storage efficiency is to improve cathode materials with high specific capacity [2]. Layered cathode materials Li[Ni$_x$Mn$_y$Co$_z$]O$_2$ (NMCs; x + y + z = 1) are successfully commercialized cathode materials [3]. Ni-rich NMC materials can provide higher energy density [3], but the application of Ni-rich NMCs is limited by their large capacity decay after long-term cycling [4]. One of the most important reasons is surface degradation from electrolyte attack [5]. At a highly delithiated state, the active Ni^{4+} ions are unstable and have a tendency to form NiO-like rock-salt phase on the material surface. The formed

NiO contributes to the formation of solid electrolyte interface (SEI), which increases the ion transfer resistance due to its more compact structure [6]. Moreover, dissolution of transition metal (TM) ions by HF attack can lead to more complex parasitic reactions, e.g., TM deposition on the anode surface or resistive metal fluorides on the cathode side [5].

To overcome these drawbacks, much effort has been focused on surface modification of Ni-rich cathode materials. Various kinds of metal oxides like Al_2O_3 [7,8], phosphate compounds like $Mn_3(PO_4)_2$ [9], polymer [10], etc., are applied as coating materials on cathode material surfaces. In this study, SiO_2 was chosen as a coating material because of its physical–chemical stability and scavenging effect on HF [11]. Additionally, SiO_2 is also a low-cost material that can be easily synthesized. Li et al. reported SiO_2 coating on $LiFePO_4$ (LFP); the coated LFP had better rate capability and higher capacity retention [12]. Zhang et al. reported application of SiO_2 coating on $Li_3V_2(PO_4)_3$/C; the material had improved electrochemical performance [13]. In the frame of this work, SiO_2-modified commercially available NMC622 materials were prepared through the same wet coating process, and their physicochemical properties and electrochemical performance were characterized and investigated.

2. Experiment

2.1. Material Preparation

All the tests in this work were based on commercially available cathode material from BASF, HED™ NMC622. The SiO_2 coating was formed by condensation reaction of tetraethyl orthosilicate (TEOS, 99.9%, Sigma Aldrich, St. Louis, MO, USA). The NMC622 powder was dispersed in the ethanol solution with a volume ratio of 20 μL TEOS/mL ethanol. The weight ratio of TEOS to NMC622 was 2%. After 3 h magnetic stirring and 1 h ultrasonic treatment at room temperature, the NMC622 suspension was dried at 70 ± 5 °C. The dried powder was calcined at 500 °C in air for 1 h, then SiO_2-coated NMC622 powder was obtained.

2.2. Microstructure Characterization

The concentrations of main elements, Li, Ni, Mn, Co, and Si, in coated and pristine NMC622 were determined by inductively coupled plasma optical emission spectrometry (ICP-OES), the oxygen content was analyzed by carrier gas hot extraction (HE), and the carbon content was identified by carbon/sulfur analyzer. The phase of samples was identified by X-ray diffraction (XRD) on X'pert PRO (PANalytical) with a Cu Kα radiation (λ = 1.54060 Å). The XRD patterns were collected in the 2θ range of 3–120° with a step size of 0.0334225°, 400.05 s time per step, and a scan speed of 0.01061 °/s. The β irradiation was eliminated by Ni-filter. The lattice constants were calculated by using HighScore software. The specimen displacement, multiple peak shape, and unit cell parameters were refined through Rietveld refinement. For phase ID determination, single peaks profile and non-phase peak fitting were used. For background determination, polynomial was used applied. The standard deviation was obtained by counting statistics, and the error of a refined value was calculated from the determinant of the inverse matrix M. (For values derived from refined parameters, the full covariance was taken into account.) The morphology of SiO_2-coated and uncoated NMC622 powders was investigated on a scanning electron microscope (SEM, Supra 40, Carl Zeiss AG, Germany). Local elemental distribution was analyzed by an energy dispersive X-ray spectroscopy (EDX, EDAX Inc., Mahwah, NJ, USA). The coating layer and its morphology were investigated by transmission electron microscopy (TEM, TECNAI F20, FEI Company, Hillsboro, OR, USA).

2.3. Electrochemical Measurement

After drying at 120 °C for 2 h, active material (AM, pristine and SiO_2-coated NMC622 powders) and carbon black (CB) were premixed manually in an agate mortar, then a part of 7 wt.% polyvinylidene fluoride (PVDF, SOLEF 5130/1001) *N*-Methyl pyrrolidone (NMP) solution was dropped in it and kneaded. After the mixture became a dough-form, it was transferred to a glass beaker, and the rest

PVDF-NMP solution was added. The mass ratio of NMC622, CB, and PVDF was 90:5:5, and the solid content of the slurry was 55 wt.%. The slurry was stirred magnetically for 12 h. This final slurry was coated on a 15-μm-thick aluminum current collector through doctor blade with a gap thickness of 90 μm and dried at 60 °C in the air for 30 min. Subsequently, the dried cathode film was transferred into a vacuum oven at 120 °C for 2 h to remove the NMP solvent completely. The electrode was calendared at 100 °C and its thickness was reduced by 10%. Through calculation [14], the film porosity decreased from uncalendared 55% ± 2% down to 48% ± 2%.

The calendared electrodes (90 mm * 200 mm) of the pristine and the SiO_2-coated NMC622 was punched into 40 pieces of 15.0 mm diameter circular electrodes. All the electrodes applied in this work had similar parameters, the areal capacity loading of AM was 1.1 ± 0.1 mAh/cm^2, based on a material loading of 7.0 ± 0.5 mg/cm^2 and a specific AM capacity of 160 mAh/g. CR2016 button cells were assembled in an argon-filled glove box from MBRAUN, whose water and oxygen content were both <0.1 ppm.

NMC622 electrode as the cathode, microporous polypropylene membrane (Celgard 2500) as the separator, and Li metal as the anode, together with one spacer and spring, were placed into the CR2016 button cells, where the electrolyte was 1 M $LiPF_6$ dissolved in ethylene carbonate (EC):ethyl methyl carbonate (EMC) = 3:7 in weight, and 2% vinylene carbonate (VC) as additive (SoulBrain).

The charge–discharge and rate capability measurements (with discharge rate of 0.1 C, 0.2 C, 0.5 C, 1 C and 2 C) were carried out on Maccor series 4000 battery tester in CCCV mode (constant current constant voltage, with a cutoff current of 10% charge current), cyclic voltammetry (CV), and electrochemical impedance spectroscopy (EIS) were performed on BioLogic VSP electrochemical workstation. After a long-term cycling, the cells were disassembled in the glove box, electrodes were washed with EMC, and studied with XRD and SEM.

3. Results and Discussion

3.1. Material Characterization

The elemental analysis results are presented in Table 1. The main element contents in the SiO_2-coated NMC622 powder remained unchanged after calcination at 500 °C. Si concentration was very close to theoretical calculation results, 0.270 wt.%, and C content did not increase–which means the expected reaction, the transformation from TEOS to SiO_2, was completed.

Table 1. Elemental analysis results of pristine and SiO_2-coated NMC622 material by ICP-OES, HE, and C/S analyzer.

Sample	Li	Ni	Mn	Co	O	Si	C
Pristine NMC622	7.17 ± 0.18	35.05 ± 0.60	10.83 ± 0.23	12.29 ± 0.26	34.6 ± 3.0	<0.005	0.0876 ± 0.0069
SiO_2-coated NMC622	7.18 ± 0.18	34.85 ± 0.59	10.79 ± 0.23	12.27 ± 0.26	33.9 ± 2.9	0.263 ± 0.011	0.0605 ± 0.0048

Unit of data: wt.%.

The XRD patterns of the pristine and coated NMC622 materials in a range of 10–80° are presented in Figure 1. All the main reflexes are indexed and coincide well to the R$\bar{3}$ m space group. Both diagrams display a single phase with α-$NaFeO_2$ structure. The reflexes of (006)/(102) and (108)/(110) split obviously, indicating that both samples are highly crystallized with layered structure. The lattice parameters, obtained through Rietveld refinement with fitting range between 3–120°, are shown in Table 2. The r_1 factor, defined by $(I_{006} + I_{102})/I_{101}$, is an indicator of the hexagonal ordering; $r_1 < 0.6$ shows a well-defined hexagonal ordering [15]. The I_{003}/I_{104} factor indicates the cation mixing in the lattice of NMC622 material; $I_{003}/I_{104} > 1.2$ is an index of no obvious cation mixing [16]. The lattice parameters were calculated by fitting the measured curves, and the lower R factors (R_{wp}, R_p) and χ^2 confirm the refinement results are reliable. The lattice parameters of the coated material did not change

significantly compared to that of the pristine ones. Additionally, no reflexes from SiO_2 were detected because of the low amount of SiO_2 coating and amorphous structure [12]. All the analysis results of XRD imply that the layered structure of NMC622 powder did not change after SiO_2 coating.
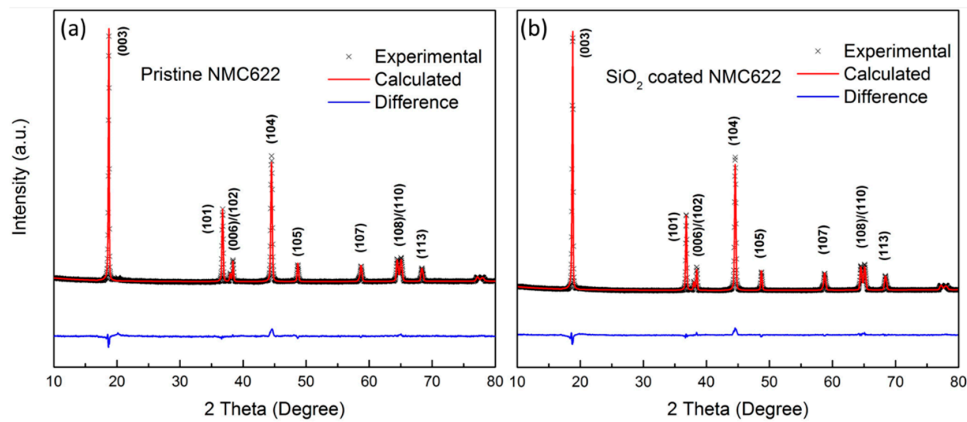

Figure 1. XRD patterns of (**a**) pristine and (**b**) SiO_2-coated NMC622 powders and their Rietveld refinement results.

Table 2. Lattice parameters and cation mixing indicators of pristine and SiO_2-coated NMC622 powders.

Sample	a (Å)	c (Å)	c/a	V (Å^3)	I_{003}/I_{104}	r_1	R_p (%)	X^2	R_{wp} (%)
Pristine NMC622	2.8666 (8)	14.222 (8)	4.961 (4)	101.22 (1)	1.690	0.497	0.647	5.76	0.996
SiO_2-coated NMC622	2.8671 (2)	14.220 (1)	4.959 (7)	101.23 (4)	1.731	0.491	0..668	4.79	1.045

Figure 2 shows the surface morphology of the pristine and the SiO_2-coated NMC622 particles at different magnifications. Approximately 200–500 nm primary NMC622 particles with rough surface formed secondary spherical particles whose size is distributed in 5–15 μm compactly. After SiO_2 coating, the NMC622 particles were covered by nano-sized particles which were formed by SiO_2, especially the boundaries between primary particles. The SiO_2-coated NMC622 particles were analyzed further in TEM (Figure 3). A 30–50 nm thin layer was formed on the particle surface after SiO_2 coating. The existence of Si is determined through elemental mapping with EDX suggests that the expected SiO_2 coating was successful.
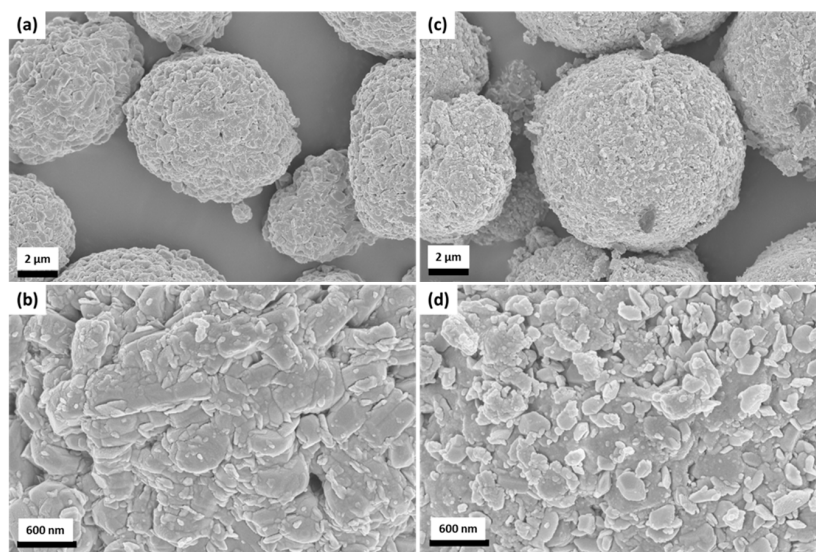

Figure 2. SEM images of (**a**,**b**) pristine and (**c**,**d**) SiO_2-coated NMC622 particles in different magnification.
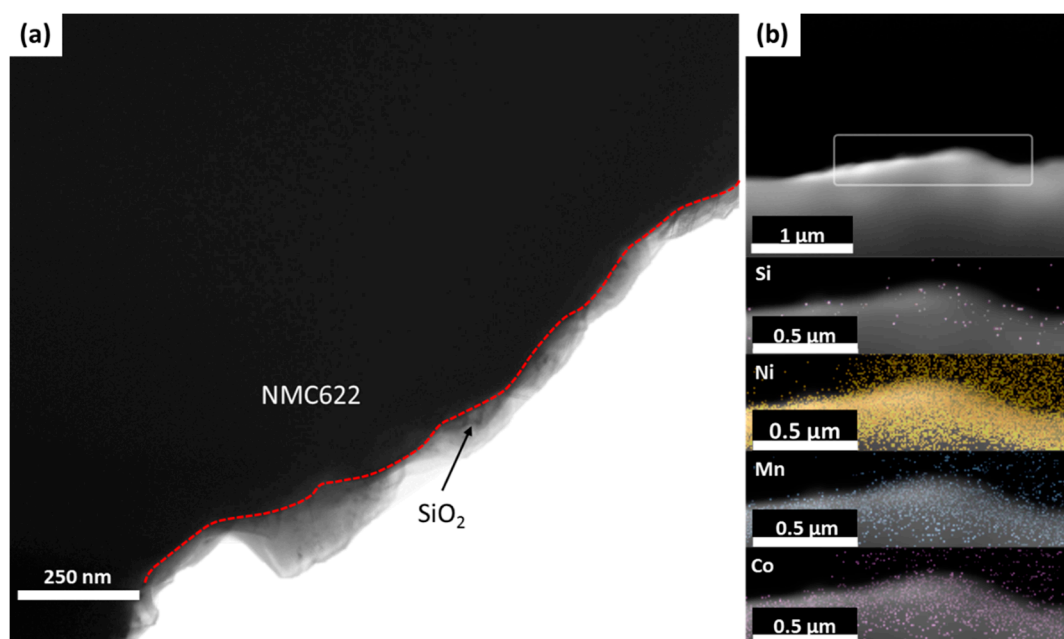
Figure 3. TEM images of (**a**) SiO$_2$-coated NMC622 particle edge and (**b**) elemental mapping by EDX.

3.2. Electrochemical Measurement

Figure 4 shows the cyclic voltammetry of the pristine and SiO$_2$-coated NMC622 electrodes in the measured voltage range of 3.0–4.3 V vs. Li/Li+ with a scan rate of 0.05 mV/s. Only one oxidation peak and one reduction peak are observed. This implies that SiO$_2$ coating is electrochemically inactive in the testing voltage range. The first oxidation peak of both sample is found at a higher potential (approximately 0.1 V) compared to the following peaks, which indicates the irreversible reactions during the initial cycle. The oxidation peak of the SiO$_2$-coated NMC622 electrode shows a slighter less shift (from 3.85 to 3.78 V) compared to that of the pristine NMC622 electrode (from 3.99 to 3.84 V) after the first cycle.
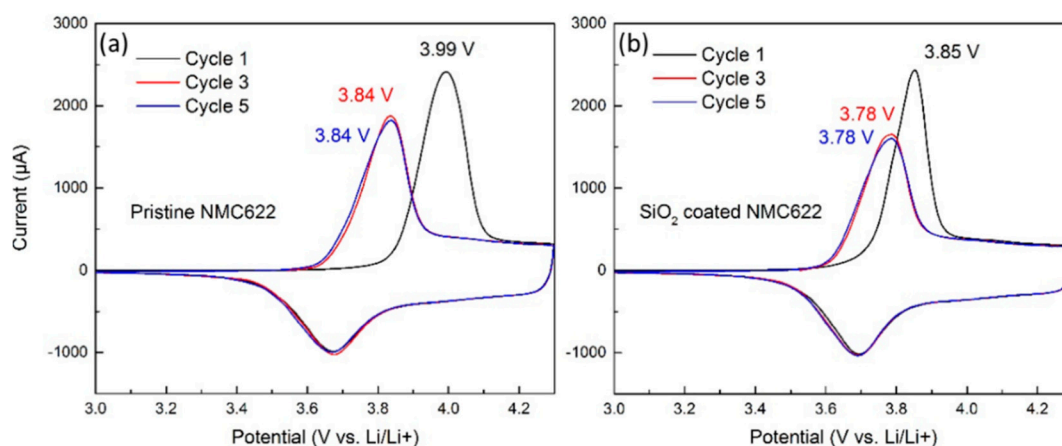
Figure 4. CV curves of (**a**) pristine and (**b**) SiO$_2$-coated NMC622 electrodes.

Figure 5 compares the rate capability of the pristine and the SiO$_2$-coated NMC622 samples with discharge rates of 0.1 C, 0.2 C, 0.5 C, 1 C, and 2 C (the specific capacity is shown in Figure S1). The NMC622 material initially had outstanding rate performance, compared to 0.1 C, at 2 C and maintained 84% of its initial capacity with excellent reproducibility. The SiO$_2$ coating layer did not deteriorate the rate capability of the NMC622 material, as the amorphous SiO$_2$ coating layer probably

allowed the pass of Li-ions because of its lower dense network structure, which did not significantly affect the ionic conductivity.
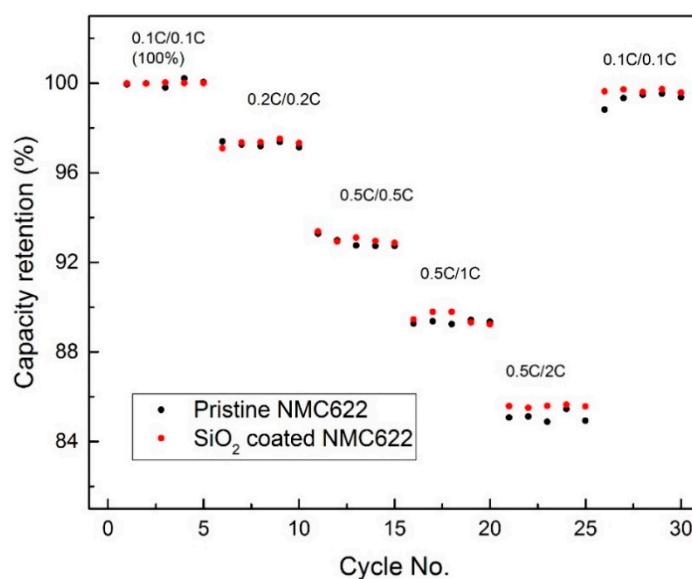

Figure 5. Comparison of rate capability between pristine and SiO$_2$-coated NMC622.

The cycling performance of the pristine and SiO$_2$-coated NMC622 electrodes is shown in Figure 6. Long-term cycling measurements were set in the voltage range of 3.0–4.3 V with 0.05 C (1 C = 160 mA/g) for formation. After five cycles at 0.05 C, a long-term cycling test was performed under 0.5 C for CCCV-charging (CV till 0.05 C) and 2.0 C for CC-discharging. As expected, both types of materials were able to be cycled for a long term. An obviously improved capacity retention of above 80% after 700 cycles was observed for SiO$_2$-coated NMC622 material, compared to pristine NMC622 which was only 74%. For the pristine NMC622 material, its capacity decreased sharply within the first 200 cycles, which implies that the most material degradation happens there. However, for the SiO$_2$-coated NMC622 material, the decreasing rate of capacity retention was constant. Figure 6b,c illustrates charge–discharge curves of the initial, 1st, 100th, 300th, and 700th cycle. Both samples show similar voltage profiles without any additional plateaus. After the first 100 cycles, the discharge potential plateau of the coated one did not decrease obviously, while the pristine one had an obvious decrease of approximately 0.3 V (the decreasing is shown by blue arrows). Furthermore, the CV (constant voltage) part percentage of the pristine NMC622 material increased from 1.3 to 12.4% after 700 cycles, while that of NMC622 with SiO$_2$ coating from 1.1 to 6.8%. This implies that the pristine NMC622 has higher polarization than the coated one. SiO$_2$ can react with HF in the electrolyte, namely preventing a series of HF-involved side-reactions, which leads to dissolution of TM [6]. Therefore, it is assumed that SiO$_2$ coating can effectively prevent NMC622 material surface degradation.

After 700 cycles, the EIS measurement was done, which was tested after discharging (the open circuit voltage was approximately 3.7 V) in a frequency range of 500 kHz–100 mHz. The Nyquist plots of both pristine and SiO$_2$-coated NMC622 cells after 700 cycles are shown in Figure 7, and the EIS at initial cycle is shown in Figure S2 as reference. The patterns of both samples are similar and consist of two semicircles. The semicircle at the high-to-medium frequency domain describes the resistance of the cathode surface film (R$_{sf}$) and the corresponding constant phase element (C$_{sf}$), while the semicircle at the low frequency range reflects the charge transfer resistance of electrochemical reactions (R$_{ct}$) and the corresponding constant phase element (C$_{ct}$). R$_s$ stands for the resistance of circuit elements (electrolyte, current collectors, electrode leads, etc.), and L for the inductance of the current collector and cable in the circuit. Warburg impedance (W) describes semi-infinite linear diffusion [17]. The equivalent circuit in Figure 7b was used to fit the EIS data, and the results are shown in Table 3, where χ^2 is the deviation

indicator. Because the SiO$_2$ coating layer is electrically isolating, a slightly higher R$_{sf}$ in the SiO$_2$-coated NMC622 is seen. It is obvious that the second semicircle, charge transfer resistance, contributes the major part of the total impedance. Specifically, in pristine NMC622 material, the surface degradation due to the formation of thicker SEI leads to a higher resistance to ionic diffusion, which affects the insertion/extraction Li-ions. It could also explain the reduced discharge potential plateau in the above charge–discharge curve (Figure 6). Totally, the resistance of SiO$_2$ coated NMC622 did not increase, that confirms the conclusions drawn from the rate capability test (Figure 5).
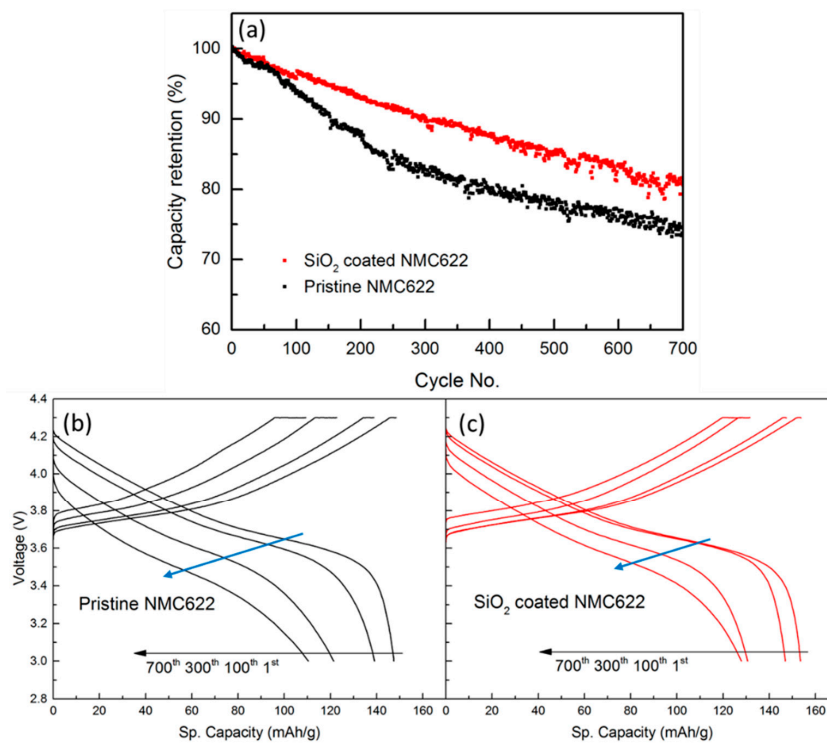
Figure 6. Cycling performance of electrode from pristine and SiO$_2$-coated NMC622: (**a**) Capacity retention, and the charge–discharge curve of (**b**) pristine NMC622 and (**c**) SiO$_2$-coated NMC622. The arrows show the discharge potential plateau decreasing.
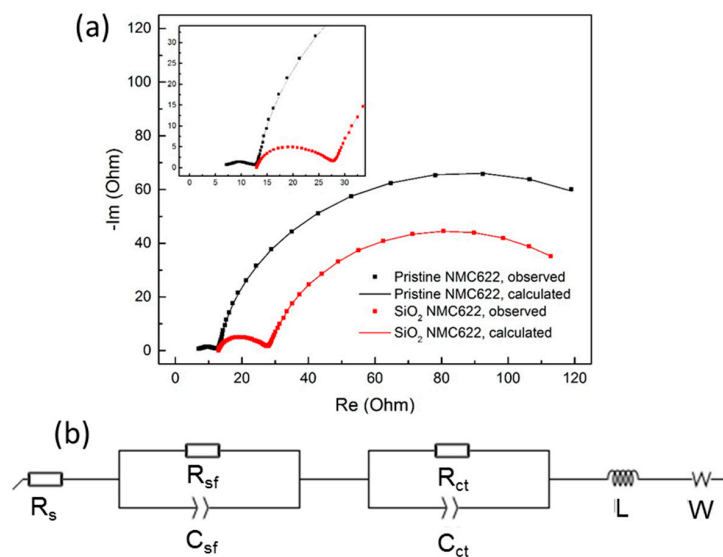

Figure 7. EIS measurements of the pristine and SiO$_2$-coated NMC622: (**a**) Nyquist plots of both samples after 700 cycles and the fitting results; (**b**) the applied equivalent circuit model [17].

Table 3. EIS fitting results of the pristine and the SiO$_2$-coated NMC622 after 700 cycles.

Sample	R$_s$ (Ω)	R$_{sf}$ (Ω)	R$_{ct}$ (Ω)	C$_f$ (F/cm^2)	C$_{ct}$ (F/cm^2)	L (H)	W (Ω·s$^{-1/2}$)	X^2
Pristine NMC622	6.279	6.875	149.400	5.45 e-4	6.24 e-3	7.484 e-9	0.093	1.41
SiO$_2$-coated NMC622	12.500	15.720	107.200	5.30 e-5	6.42 e-3	1.160 e-7	6.387	5.43

3.3. Post-Mortem Analysis

After 700 cycles, both cells were disassembled in a glove box, and the electrodes were washed with EMC. The electrodes were observed visually at first, and no defect, delamination, or crack was found (Figure S2).

The electrodes were further investigated in SEM by applying different magnifications (Figure 8). The images of lower magnification do not show any difference: Particles stack compactly, and particle surface is adhered by nano-sized carbon black. At higher magnification, some intergranular cracks on the particle surface of the pristine NMC622 are found, but none on the SiO$_2$-coated one. On the pristine NMC622 material, the formation of intergranular cracks among the primary particles in the secondary particles was resulted from the anisotropic volume change due to Li-ionic (de)intercalation during charging and discharging, while the volume change was restricted by the SiO$_2$ layer. Moreover, the generated cracks expose more internal surface of the pristine NMC622 particles to electrolyte, which accelerate the side-reactions and consume capacity [6,18]. SiO$_2$ as HF scavenger can reduce side-reactions and retain the stable layered structure. Therefore, no obvious cracks could be found on the surface. This is further proof for the above explanation of the higher capacity retention of SiO$_2$-coated NMC622.
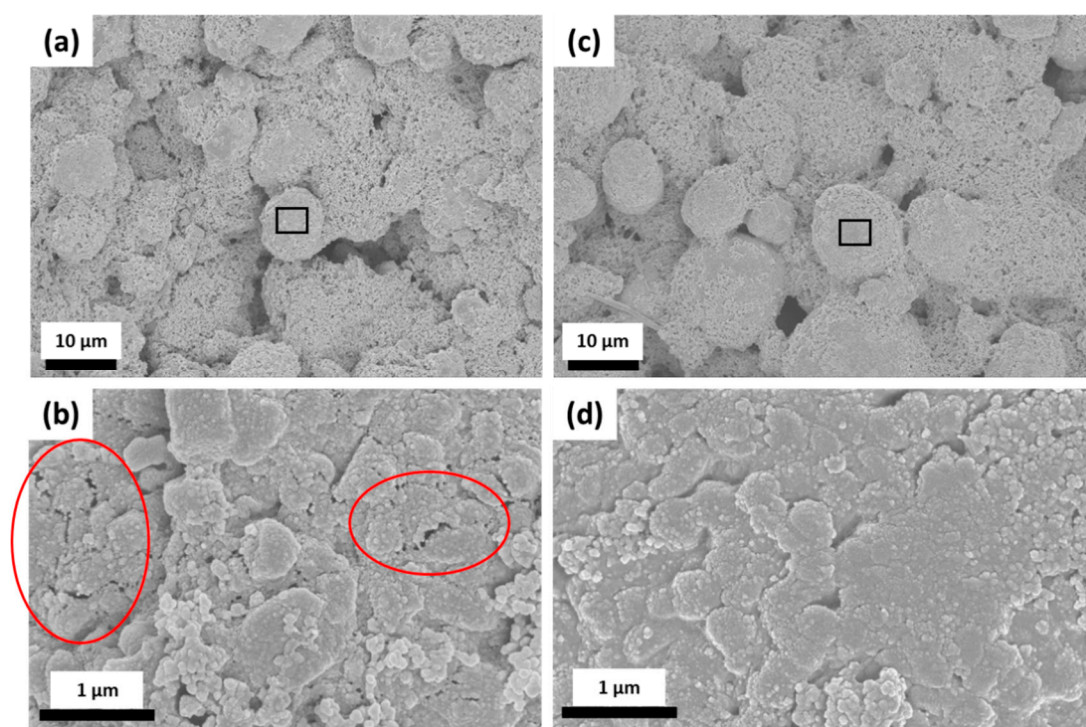
Figure 8. SEM images for cycled Electrode: (**a**,**b**) Pristine (**c**,**d**) SiO$_2$-coated NMC622.

The electrodes were placed in a special airtight argon-filled specimen holder and measured with XRD. In Figure 9, compared to an uncycled pristine NMC622 electrode, slight deviation (till 0.3°) of the reflexes position is detected. On the one hand, the shifting to the left reveals the higher c parameter, because more lithium ions could insert into the SiO$_2$-coated NMC622 material than the

pristine one, and the lithium slab is thicker. On the other hand, the measured sample is uneven electrode, which could lead to deviation of result. An extra reflex at 65° is from Al-current collector. The determination of full width of half maximum (FWHM) of main reflexes shown in Table S1 reveals that the SiO$_2$-coated NMC622 electrode has sharper reflexes than the pristine one, which indicates a better crystallinity. The reason behind it could be homogenous crystal structure because of less-exposed surface. According to the Scherrer formula

$$L = \frac{K \cdot \lambda}{\beta \cdot \cos \theta}$$

where β is the width of Bragg line in radians (here is FWHM), K is a shape factor 0.9, λ is the wavelength of the X-ray, θ is the corresponding Bragg angle, reflexes with decreased width indicate larger mean crystallites [16], the calculated mean crystallite size is shown in Table 4.
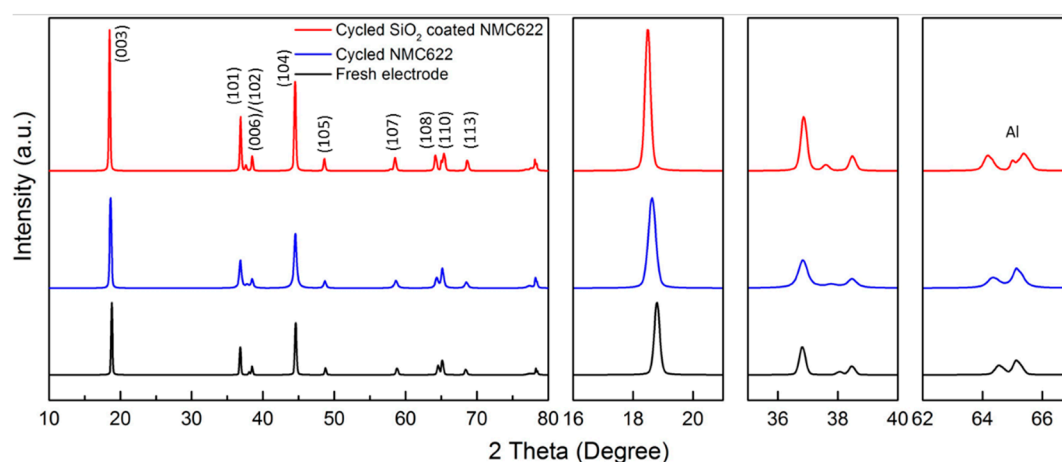
Figure 9. Ex-situ XRD of the pristine and SiO$_2$-coated NMC622 electrodes after 700 cycles.

Table 4. The crystallite size obtained by calculation of full width of half maximum (FWHM).

Sample	Uncycled Pristine NMC622	Cycled Pristine NMC622	Cycled SiO$_2$-Coated NMC622
Crystallite size (Å)	470 ± 48	253 ± 72	452 ± 54

4. Conclusions

In this work, the wet coating method was applied on a commercialized NMC622 material for the first time, and a significant improvement of electrochemical performance was obtained. It was shown that the long-term cyclability of commercial NMC622 was significantly enhanced, even at relatively higher discharge rates (2 C), via a simple coating method. This can increase the cycle life of commercially available Li-Ion batteries without decreasing their rate performance. An amorphous SiO$_2$ layer was formed on the NMC622 material surface successfully, which did not change the base material due to the coating process. The SiO$_2$ coating layer can reduce the side reactions between material surface and the electrolyte, especially at the first 200 cycles, where most capacity fading occurs. The capacity retention of coated NMC622 is visibly improved even after up to 700 cycles. EIS measurement shows that the SiO$_2$-coated material has less charge transfer resistance. XRD patterns reveal that after long-term cycling, NMC622 with an SiO$_2$ coating layer still has very good crystallinity. Compared to previous work [9,12,13] the application of SiO$_2$ coating on synthesized NMC622 did not show obvious improvement in the first 50 cycles, but the coating method is still beneficial for long-term cycling. To summarize, SiO$_2$ coating is an effective and facile surface modification method, even for commercialized NMC622 material, for long-term cycle capability and therefore longer service life.

References

1. Wood, D.L., III; Li, J.; Daniel, C. Prospects for reducing the processing coast of lithium ion batteries. *J. Power Sour.* **2015**, *275*, 234–242. [CrossRef]

2. Ding, Y.; Cano, Z.P.; Yu, A.; Lu, J.; Chen, Z. Automotive Li-ion batteries: Current status and future perspectives. *Electrochem. Energy Rev.* **2019**, *2*, 1–28. [CrossRef]

3. Andre, D.; Kim, S.J.; Lamp, P.; Lux, S.F.; Maglia, F.; Paschos, O.; Stiaszny, B. Future generations of cathode materials: An automative industry perspective. *J. Mater. Chem. A* **2015**, *3*, 6709–6732. [CrossRef]

4. Noh, H.J.; Youn, S.; Yoon, C.S.; Sun, Y.K. Comparison of the structural and electrochemical properties of layered Li[Ni$_x$Co$_y$Mn$_z$]O$_2$ (x = 1/3, 0.5, 0.6, 0.7, 0.8, and 0.85) cathode material for lithium-ion batteries. *J. Power Sour.* **2013**, *233*, 121–130. [CrossRef]

5. Han, J.G.; Kim, K.; Lee, Y.; Choi, N.S. Scavenging materials to stabilize LiPF$_6$-containing carbonate-based electrolytes for Li-ion batteries. *Adv. Mater.* **2018**, *31*, 1804822. [CrossRef] [PubMed]

6. Ryu, H.H.; Park, K.J.; Yoon, C.S.; Sun, Y.K. Capacity fading of ni-rich Li[Ni$_x$Co$_y$Mn$_{1-x-y}$]O$_2$ (0.6 ≤ x ≤ 0.95) cathodes for high-energy-density lithium-ion batteries: Bulk or surface degradation? *Chem. Mater.* **2018**, *30*, 1155–1163. [CrossRef]

7. Wise, A.M.; Ban, C.; Weker, J.N.; Misra, S.; Cavanagh, A.S.; Wu, Z.; Li, Z.; Whittingham, M.S.; Xu, K.; George, S.M.; et al. Effect of Al$_2$O$_3$ coating on stabilizing LiNi$_{0.4}$Mn$_{0.4}$Co$_{0.2}$O$_2$ cathodes. *Chem. Mater.* **2015**, *27*, 6146–6154. [CrossRef]

8. Neudeck, S.; Strauss, F.; Garcia, G.; Wolf, H.; Janek, J.; Harmann, P.; Brezesinski, T. Room temperature, liquid-phase Al$_2$O$_3$ surface. *Chem. Commun.* **2019**, *55*, 2174–2177. [CrossRef] [PubMed]

9. Cho, W.; Kim, S.M.; Lee, K.W.; Song, J.H.; Jo, Y.N.; Kim, H.; Kim, J.S.; Kim, Y.J. Investigation of new manganese orthophosphate Mn$_3$(PO$_4$)$_2$ coating for nickel-rich LiNi$_{0.6}$Co$_{0.2}$Mn$_{0.2}$O$_2$ cathode and improvement of its thermal properties. *Electrochim. Acta* **2016**, *198*, 77–83. [CrossRef]

10. Cao, Y.; Qi, X.; Hu, K.; Wang, Y.; Gan, Z.; Li, Y.; Hu, G.; Peng, Z.; Du, K. Conductive polymers encapsulation to enhance electrochemical performance of Ni-rich cathode materials for Li-ion batteries. *ACS Appl. Mater. Interfaces* **2018**, *10*, 18270–18280. [CrossRef] [PubMed]

11. Cho, W.; Kim, S.M.; Song, J.H.; Yim, T.; Woo, S.G.; Lee, K.W.; Kim, J.S.; Kim, Y.J. Improved electrochemical and thermal properties of nickel rich LiNi$_{0.6}$Co$_{0.2}$Mn$_{0.2}$O$_2$ cathode materials by SiO$_2$ coating. *J. Power Sour.* **2015**, *282*, 45–50. [CrossRef]

12. Li, Y.D.; Zhao, S.X.; Nan, C.W.; Li, B.H. Electrochemical performance of SiO$_2$-coated LiFePO$_4$ cathode materials for lithium ion battery. *J. Alloy. Compd.* **2011**, *509*, 957–960. [CrossRef]

13. Zhang, L.L.; Liang, G.; Peng, G.; Zou, F.; Huang, Y.H.; Croft, M.C. Significantly improved electrochemical performance in Li$_3$V$_2$(PO$_4$)$_3$/C Promoted by SiO$_2$ coating for lithium-ion batteries. *J. Phys. Chem. C* **2012**, *116*, 12401–12408. [CrossRef]

14. Zheng, H.; Yang, R.; Liu, G.; Song, X.; Battaglia, V.S. Cooperation between active material, polymeric binder and conductive carbon additive in lithium ion battery cathode. *J. Phys. Chem. C* **2012**, *116*, 4875–4882. [CrossRef]

15. Periasamy, P.; Kalaiselvi, N.; Kim, H. High voltage and high capacity characteristics of $LiNi_{1/3}Co_{1/3}Mn_{1/3}O_2$ cathode for lithium battery applications. *Int. J. Electrochem. Sci.* **2007**, *2*, 689–699.

16. Zhang, X.; Jiang, W.; Mauger, A.; Qilu; Gendron, F.; Julien, C. Minimization of the cation mixing in $Li_{1+x}(NMC)_{1-x}O_2$ as cathode material. *J. Power Sour.* **2010**, *195*, 1292–1301. [CrossRef]

17. Liang, L.; Hu, G.; Jiang, F.; Cao, Y. Electrochemical behaviors of SiO_2-coated $LiNi_{0.8}Co_{0.1}Mn_{0.1}O_2$. *J. Alloy. Compd.* **2016**, *657*, 570–581. [CrossRef]

18. Ruan, Y.; Song, X.; Fu, Y.; Song, C.; Battaglia, V. Structural evolution and capacity degradation mechanism of $LiNi_{0.6}Mn_{0.2}Co_{0.2}O_2$ cathode materials. *J. Power Sour.* **2018**, *400*, 539–548. [CrossRef]